

## A 2D Pseudo-Spectral Approach of Photonic Crystal Slabs

K. Varis<sup>(a)</sup>, and A. R. Baghai-Wadji<sup>(b)</sup>

<sup>(a)</sup>Helsinki University of Technology, Optoelectronics Laboratory,  
P.O. Box 3000, FIN-02015 HUT, Finland, EU  
karri.varis@hut.fi

<sup>(b)</sup>Vienna University of Technology, E366,  
Gusshausstrasse 27-29, A-1040 Vienna, Austria, EU  
alireza.baghai-wadji@tuwien.ac.at

**Abstract**— We consider an  $L_1$ -periodic dielectric slab which is characterized by the dielectric function  $\varepsilon(x + L_1, z) = \varepsilon(x, z)$  as a 2D model for photonic crystals. We assume that there is no variation in  $y$ -direction, with fields varying time-harmonically according to  $\exp(-j\omega t)$ . In order to solve electromagnetic wave propagation in such structures, we diagonalize the Maxwell's equations with respect to the  $z$ -coordinate. As demonstrated in this paper, diagonalized forms greatly facilitate the implementation of the finite difference method. The  $L_1$ -periodicity of the fields suggests expansions in terms of spatially harmonic functions. However, contrary to the commonly-used Bloch inhomogeneous plane waves, we utilize expansions of the form  $\psi(x, z) = \sum_{n=0}^{N-1} \psi_n(z) \exp[j(k_n + K)x]$ . For the determination of the coefficient functions  $\psi_n(z)$  we employ a sophisticated, yet, easy-to-apply implementation of a finite difference discretization scheme in the  $z$ -direction which permits virtually arbitrary  $L_1$ -periodic  $\varepsilon(x, z)$  profile functions. It will be demonstrated that the proposed hybridization of the plane-wave decomposition and the finite difference method leads to a robust and flexible method of analysis with a wide range of applications. As an example, we consider TE-polarized electromagnetic waves which propagate in the assumed dielectric slab along the  $x$ -axis.

### I. INTRODUCTION

We consider an  $L_1$ -periodic dielectric slab characterized by the permittivity function  $\varepsilon(x + L_1, z) = \varepsilon(x, z)$  as a 2D model for photonic crystals. We assume that there is no variation in  $y$ -direction, with fields varying time-harmonically according to  $\exp(-j\omega t)$ . We present a general scheme for the diagonalization of Maxwell's equations with respect to the  $z$ -coordinate and consider TE-polarized electromagnetic waves propagating in the assumed dielectric slab along the  $x$ -axis. The  $L_1$ -periodicity of the fields suggests expansions in terms of spatially harmonic functions. However, contrary to the commonly-used Bloch inhomogeneous plane waves, we utilize expansions of the form  $\psi(x, z) = \sum_{n=0}^{N-1} \psi_n(z) \exp[j(k_n + K)x]$ . For the determination of the coefficient functions  $\psi_n(z)$  we employ a sophisticated, yet, easy-to-apply implementation of a finite difference discretization scheme in  $z$ -direction which permits virtually arbitrary permit-

tivity profile functions  $\varepsilon(x, z)$ . It will be demonstrated that the proposed hybridization of the plane-wave decomposition and the finite difference method leads to a robust and flexible method of analysis with a wide range of applications.

Contrary to the standard finite difference implementations which include the entirety of the  $\mathbf{E}$ - and  $\mathbf{H}$ -components, in our technique, we use an FD discretization, which only involves an "optimized subset" of the field components [1,2]. Stated more precisely, only those field components are involved in our formalism, which enter the interface- or boundary conditions on  $z = \text{const}$  planes: It turns out that these "transversal" field components are the only unknowns in our problems; the remaining "normal" components can be uniquely determined once the transversal fields have been calculated.

This paper is organized as follows: In Section II. we briefly comment on the diagonalization procedure. The electromagnetic wave propagating in a photonic crystal, as specified above, decouples into a TE- and a TM-polarized mode. In this paper we focus on TE-modes. In Section III. we discuss the discretization and approximation of the fields. Section IV. is devoted to formulating appropriate boundary conditions for our problem. Thereby, assuming free space below and above our structure, we formulate discrete boundary conditions in a matrix form. Section V. is devoted to the specifics of our numerical calculations. We discuss tools and measures which we have developed to enhance the speed, and at the same time, the accuracy of our computations. In Section VI. we discuss a glimpse of the numerical results which we have obtained. We compare our results with available data. Section VII. concludes our discussion.

**Notation:** In the following we exploit the  $L_1$ -periodicity property and assume that the real-valued variable  $K$  (to be specified soon) varies in the interval  $[-\pi/L_1, \pi/L_1]$ . Furthermore, we have defined

$$k_n = \begin{cases} \frac{2\pi}{L_1} n & 0 \leq n \leq \frac{N}{2} \\ \frac{2\pi}{L_1} (n - N) & \frac{N}{2} < n \leq N - 1 \end{cases} \quad (1)$$

## II. DIAGONALIZATION

Consider the Maxwell's curl equations under the following two assumptions: (i) no variation in  $y$ -direction ( $\partial_y \equiv 0$ ), and (ii) isotropic materials specified by a constant permeability  $\mu$ , and an  $L_1$ -periodic inhomogeneous permittivity function  $\varepsilon(x, z)$ :  $\varepsilon(x + L_1, z) = \varepsilon(x, z)$ . Assumptions (i) and (ii) imply the constitutive equations in the forms  $\mathbf{B} = \mu\mathbf{H}$  and  $\mathbf{D} = \varepsilon(x, z)\mathbf{E}$ . Consequently, Maxwell's equations are:

$$-\partial_x \begin{bmatrix} 1 \\ 0 \end{bmatrix} H_3 + \partial_z \begin{pmatrix} H_1 \\ H_2 \end{pmatrix} = -j\omega\varepsilon(x, z) \begin{pmatrix} E_2 \\ -E_1 \end{pmatrix} \quad (2a)$$

$$-\partial_x \begin{bmatrix} 1 \\ 0 \end{bmatrix} E_3 + \partial_z \begin{pmatrix} E_1 \\ E_2 \end{pmatrix} = j\omega\mu \begin{pmatrix} H_2 \\ -H_1 \end{pmatrix} \quad (2b)$$

$$\partial_x H_2 = -j\omega\varepsilon(x, z)E_3 \quad (2c)$$

$$\partial_x E_2 = j\omega\mu H_3. \quad (2d)$$

Our goal is the diagonalization of (2) with respect to the  $z$ -axis. In other words, we are aiming at an equation of the form:  $\mathcal{L}(x, z)\tilde{\psi} = \partial_z\tilde{\psi}$ . Equations (2a) and (2b) can be written in the form:

$$\begin{pmatrix} 0 & 0 & 0 & j\omega\mu \\ 0 & 0 & -j\omega\mu & 0 \\ 0 & -j\omega\varepsilon(x, z) & 0 & 0 \\ j\omega\varepsilon(x, z) & 0 & 0 & 0 \end{pmatrix} \begin{pmatrix} E_1 \\ E_2 \\ H_1 \\ H_2 \end{pmatrix} + \begin{pmatrix} \partial_x & 0 \\ 0 & 0 \\ 0 & \partial_x \\ 0 & 0 \end{pmatrix} \begin{pmatrix} E_3 \\ H_3 \end{pmatrix} = \partial_z \begin{pmatrix} E_1 \\ E_2 \\ H_1 \\ H_2 \end{pmatrix}, \quad (3)$$

while (2c) and (2d) give:

$$\begin{pmatrix} E_3 \\ H_3 \end{pmatrix} = \begin{pmatrix} 0 & 0 \\ 0 & \frac{\partial_x}{j\omega\mu} \\ 0 & 0 \\ -\frac{\partial_x}{j\omega\varepsilon(x, z)} & 0 \end{pmatrix}^T \begin{pmatrix} E_1 \\ E_2 \\ H_1 \\ H_2 \end{pmatrix}. \quad (4)$$

Substituting (4) into (3) we obtain the desired diagonalized form, which can be written in the form  $\mathcal{L}(x, z)\tilde{\psi} = \partial_z\tilde{\psi}$ . Note that the  $z$ -dependence in  $\mathcal{L}(x, z)$  is due to the  $z$ -dependence in the  $\varepsilon(x, z)$  function. The differential  $\mathcal{L}(x, z)$ -operator is devoid of  $z$ -derivatives. The  $z$ -diagonalized form can be interpreted as follows: Evaluate  $\mathcal{L}(x, z)$  at a certain point  $z$ , say,  $z_0$ , to obtain  $\mathcal{L}(x, z_0)$ . Determine the expressions for  $\mathcal{L}(x, z_0)\tilde{\psi}$ . This gives the rate of change of  $\tilde{\psi}$  in the  $z$ -direction at  $z = z_0$ , i.e.  $\partial_z\tilde{\psi}$  at  $z = z_0$ . In the present case the system of equations  $\mathcal{L}(x, z)\tilde{\psi} = \partial_z\tilde{\psi}$  decouples into the following subsets:

1)  $z$ -diagonalized transversal electric fields: It is straightforward to show that the  $z$ -diagonalized transversal electric fields satisfy equation (5),

$$\begin{pmatrix} 0 & -j\omega\mu \\ -j\omega\varepsilon(x, z) + \frac{1}{j\omega\mu}\partial_x^2 & 0 \end{pmatrix} \begin{pmatrix} E_2 \\ H_1 \end{pmatrix} = \partial_z \begin{pmatrix} E_2 \\ H_1 \end{pmatrix} \quad (5a)$$

$$H_3 = \frac{1}{j\omega\mu}\partial_x E_2. \quad (5b)$$

2)  $z$ -diagonalized transversal magnetic fields: The  $z$ -diagonalized equation for the transversal magnetic fields is

$$\begin{pmatrix} 0 & j\omega\mu - \partial_x \frac{1}{j\omega\varepsilon(x, z)} \partial_x \\ j\omega\varepsilon(x, z) & 0 \end{pmatrix} \begin{pmatrix} E_1 \\ H_2 \end{pmatrix} = \partial_z \begin{pmatrix} E_1 \\ H_2 \end{pmatrix} \quad (6a)$$

$$E_3 = -\frac{1}{j\omega\varepsilon(x, z)}\partial_x H_2. \quad (6b)$$

## III. ANALYSIS OF TE-POLARIZED WAVES IN PERIODIC DIELECTRICS

In this paper we will focus on the TE-polarized waves, i.e. we consider (5), which we write in the form:

$$\left(-j\omega\varepsilon(x, z) + \frac{1}{j\omega\mu}\partial_x^2\right)E_2 = \partial_z H_1 \quad (7a)$$

$$-j\omega\mu H_1 = \partial_z E_2. \quad (7b)$$

### A. Discretization of the Fields

As will be clear in the sequel we discretize the fields in  $x$ - and  $z$ -directions differently. We exploit the periodicity conditions in  $x$ -direction and decompose the fields in spatial harmonics in this direction. However, we choose a finite difference discretization in  $z$ -direction. The following sections are devoted to the procedural details.

1) *Treatment of the  $x$ -dependence*:  $L_1$ -periodicity suggests the following approximation for the fields:

$$E_2(x, z) = \sum_{n=0}^{N-1} e_n(z) e^{j(k_n + K)x} \quad (8a)$$

$$H_1(x, z) = \sum_{n=0}^{N-1} h_n(z) e^{j(k_n + K)x}. \quad (8b)$$

For  $z = z_0 = \text{const}$  the finite sums at the RHS of (8) are infinitely differentiable with respect to  $x$ . Substitute (8) into (7). Define the linear functional  $D_m$

$$D_m(f) = \frac{1}{L_1} \int_0^{L_1} dx f(x, \cdot) e^{-j(k_m + K)x} \quad (9)$$

for  $m \in [0, N-1]$ . Apply  $D_m$  to both sides of (7). Use the fact that

$$\delta[m-n] = \frac{1}{L_1} \int_0^{L_1} dx e^{-j(k_m - k_n)x} \quad (10)$$

with  $\delta[n]$  being the Kronecker symbol, and

$$\varepsilon_{m-n}(z) = \frac{1}{L_1} \int_0^{L_1} dx \varepsilon(x, z) e^{-j(k_m - k_n)x} \quad (11)$$

to obtain

$$\frac{j}{\omega\mu} (k_m + K)^2 e_m(z) - j\omega \sum_{n=0}^{N-1} e_n(z) \varepsilon_{m-n}(z) = \partial_z h_m(z) \quad (12a)$$

$$-j\omega\mu h_m(z) = \partial_z e_m(z). \quad (12b)$$

Consider the integral representation for  $\varepsilon_{m-n}(z)$ , Eq. (11), with  $m, n \in [0, N-1]$ . Using  $k_m - k_n = \frac{2\pi}{L_1}(m-n)$  we obtain,

$$\varepsilon_{m-n}(z) = \frac{1}{L_1} \int_0^{L_1} dx \varepsilon(x, z) e^{-j\frac{2\pi}{L_1}(m-n)x}. \quad (13)$$

Observe that  $\min(m-n) = 0 - (N-1) = -N+1$  and  $\max(m-n) = (N-1) - 0 = N-1$ . Therefore, for every fixed value of  $z$  we need to evaluate Fourier integrals of the form

$$\varepsilon_l(z) = \frac{1}{L_1} \int_0^{L_1} dx \varepsilon(x, z) e^{-j\frac{2\pi}{L_1}lx} \quad (14)$$

at  $2N-1$  discrete ‘‘frequency’’ values in the range  $l \in [-N+1, N-1]$ . In our simulations we have evaluated integrals (14) by utilizing Fast Fourier Transform (FFT), and requiring  $2N-1$  sampling points  $\varepsilon(x_i, z_0)$ ;  $i \in [1, 2N-1]$  of the function  $\varepsilon(x, z_0)$  for every fix value  $z_0$  of  $z$ .

### B. Discretization in $z$ -direction

As pointed out earlier we use a finite difference discretization in  $z$ -direction. However, in contrast to the standard techniques, our implementation of the finite difference technique involves Fourier coefficients rather than the fields in real space. In what follows we

demonstrate the way how we discretize the  $z$ -dependent part of the coefficients. To this end it is advantageous to adopt the abbreviation  $f_m^i = f_m(i\Delta_z)$ . Thereby,  $f_m^i$  means the  $m^{\text{th}}$  Fourier coefficient of the function  $f(x, z)$  sampled at  $z = i\Delta_z$ . Using this notation we obtain:

$$\frac{j\Delta_z}{\omega\mu} (k_m + K)^2 e_m^{i-\frac{1}{2}} - j\omega\Delta_z \sum_{n=0}^{N-1} e_n^{i-\frac{1}{2}} \varepsilon_{m-n}^{i-\frac{1}{2}} + h_m^{i-1} = h_m^i \quad (15a)$$

$$-j\omega\mu\Delta_z h_m^i + e_m^{i-\frac{1}{2}} = e_m^{i+\frac{1}{2}}. \quad (15b)$$

These equations in the matrix form read:

$$\mathbf{A}^{i-\frac{1}{2}} \mathbf{e}^{i-\frac{1}{2}} + \mathbf{h}^{i-1} = \mathbf{h}^i \quad (16a)$$

$$\mathbf{B}^i \mathbf{h}^i + \mathbf{e}^{i-\frac{1}{2}} = \mathbf{e}^{i+\frac{1}{2}}. \quad (16b)$$

The coefficient matrices  $\mathbf{A}$  and  $\mathbf{B}$  in (16) have the following structure:

$$\mathbf{A} = -j\Delta_z \left\{ \omega\mathbf{P} - \frac{1}{\omega\mu} (\mathbf{Q} + \mathbf{K}\mathbf{I})^2 \right\} \quad (17)$$

with

$$\mathbf{P} = \begin{bmatrix} \varepsilon_0 & \varepsilon_{-1} & \varepsilon_{-2} & \cdot & \cdot & \cdot & \varepsilon_{-N+1} \\ \varepsilon_1 & \varepsilon_0 & \varepsilon_{-1} & \cdot & \cdot & \cdot & \varepsilon_{-N+2} \\ \varepsilon_2 & \varepsilon_1 & \varepsilon_0 & \cdot & \cdot & \cdot & \cdot \\ \cdot & \cdot & \cdot & \cdot & \cdot & \cdot & \cdot \\ \cdot & \cdot & \cdot & \cdot & \cdot & \cdot & \cdot \\ \cdot & \cdot & \cdot & \cdot & \cdot & \cdot & \cdot \\ \varepsilon_{N-2} & \cdot & \cdot & \cdot & \cdot & \cdot & \cdot \\ \varepsilon_{N-1} & \varepsilon_{N-2} & \cdot & \cdot & \cdot & \cdot & \varepsilon_0 \end{bmatrix} \quad (18)$$

and

$$\mathbf{Q} = \begin{bmatrix} k_0 & 0 & 0 & \cdot & \cdot & \cdot & 0 \\ 0 & k_1 & 0 & \cdot & \cdot & \cdot & 0 \\ \cdot & \cdot & \cdot & \cdot & \cdot & \cdot & \cdot \\ \cdot & \cdot & \cdot & \cdot & \cdot & \cdot & \cdot \\ \cdot & \cdot & \cdot & \cdot & \cdot & \cdot & \cdot \\ 0 & \cdot & \cdot & \cdot & \cdot & \cdot & \cdot \\ 0 & 0 & \cdot & \cdot & \cdot & \cdot & k_{N-1} \end{bmatrix} \quad (19)$$

and

$$\mathbf{B} = -j\omega\mu\Delta_z \mathbf{I}. \quad (20)$$

### C. Boundedness property of $\mathbf{P}_\infty$

For analyzing the stability of the system of equations, which we will construct in the next section, it is

imperative to investigate the properties of the involved matrices. The finite dimensional matrix  $\mathbf{P}(= \mathbf{P}_N)$  in (18) is the truncated version (projection) of an infinite dimensional matrix that we denote by  $\mathbf{P}_\infty$ . It is recognized that we are concerned with Toeplitz matrices, which considered as kernels, have rich analytical properties. It is easily seen that  $\mathbf{P}_\infty$  is uniquely determined by a two-sided infinite sequence  $\{\varepsilon_l | l = 0, \pm 1, \pm 2, \dots\}$  with  $\mathbf{P}_\infty(\mathbf{m}, \mathbf{n}) = \varepsilon_{\mathbf{m}-\mathbf{n}}$  ( $m, n = 0, 1, 2, \dots$ ).

Furthermore, we understand that for any physically realizable dielectric medium the function  $\varepsilon(x, z_i)$  is in  $L^\infty(-\pi/2, \pi/2)$ , the space of all essentially bounded functions  $f(x)$  defined on  $[-\pi/2, \pi/2]$ , which are finite in the norm  $\|f\|_\infty$ . Here  $\|f\|_\infty$  denotes the essential supremum of  $|f(x)|$ , with  $x \in [-\pi/2, \pi/2]$ .

In addition, we remember that we obtained  $\varepsilon_l$  as Fourier coefficients of  $\varepsilon(x, z)$  (evaluated at a fixed point  $z_0$ ) with respect to the functions  $e_l(x) = \exp(j2\pi lx)$ , ( $l = 0, \pm 1, \pm 2, \dots$ ). Using standard theorems in the theory of Toeplitz matrices, we can show that based on these properties  $\mathbf{P}_\infty(m, n) = \varepsilon_{m-n}$ , and thus  $\mathbf{P}_N$  are bounded.

1) *Creating the global system of equations:* The fields along the  $z$ - direction can be determined recursively by using (16) which we write in the form:

$$\mathbf{A}^{i-\frac{1}{2}} \mathbf{e}^{i-\frac{1}{2}} + \mathbf{h}^{i-1} - \mathbf{h}^i = 0 \quad (21a)$$

$$\mathbf{B}^i \mathbf{h}^i + \mathbf{e}^{i-\frac{1}{2}} - \mathbf{e}^{i+\frac{1}{2}} = 0. \quad (21b)$$

We terminate our computational grid at two bounding  $z = \text{const}$  levels: The lower bound being  $z = -\Delta_z/2$  and the upper bound being  $z = (n_z + 1/2)\Delta_z$ . Therefore, the simulation domain occupies the region  $z \in [0, n_z]\Delta_z$ . As is evident from (21) the magnetic fields are evaluated at even multiples of  $\Delta_z/2$  while the electric fields are evaluated at odd multiples of  $\Delta_z/2$ . Consequently, we need to calculate the electric fields at  $z = -\Delta_z/2$  and  $z = (n_z + 1/2)\Delta_z$ , i.e.,  $\exp(-\Delta_z/2)$  and  $\exp((n_z + 1/2)\Delta_z)$ . As will be shown in the next section these electric field values will be calculated from the field distributions in the adjacent media immediately below and above the corrugated slab. In view of (21), and with  $i$  running through the interval  $[0, n_z]$ , we can assemble the desired global system. The interlaced algorithm, which we have utilized for constructing the global system, is sketched in Fig. 1.

#### IV. BOUNDARY CONDITIONS

##### A. Open Boundary Problems

Assume free space for  $z < 0$  and  $z > n_z\Delta_z$ . In free space our diagonalized equations take a particularly simple form: For the field expansion coefficients  $e_n(z)$

$$\begin{array}{l} H_N = \Phi_u E_{N+0.5} \cdots \cdots \cdots E_{N+0.5} = E_{N-0.5} + \Delta(\partial_z E)_N \\ H_N = H_{N-1} + \Delta(\partial_z H)_{N-0.5} \cdots \cdots \cdots (\partial_z E)_N = A_N H_N \\ (\partial_z H)_{N-0.5} = B_{N-0.5} E_{N-0.5} \cdots \cdots \cdots E_{N-0.5} = E_{N-1.5} + \Delta(\partial_z E)_{N-1} \\ H_{N-1} = H_{N-2} + \Delta(\partial_z H)_{N-1.5} \cdots \cdots \cdots (\partial_z E)_{N-1} = A_{N-1} H_{N-1} \\ \vdots \\ H_1 = H_0 + \Delta(\partial_z H)_{0.5} \cdots \cdots \cdots (\partial_z E)_1 = A_1 H_1 \\ (\partial_z H)_{0.5} = B_{0.5} E_{0.5} \cdots \cdots \cdots E_{0.5} = E_{-0.5} + \Delta(\partial_z E)_0 \\ H_0 = \Phi_l E_{-0.5} \cdots \cdots \cdots (\partial_z E)_0 = A_0 H_0 \\ \vdots \\ \cdots \cdots \cdots E_{-0.5} \end{array}$$

Fig. 1. A representation of how electric and magnetic fields are defined on interlaced layers. The text at the LHS should describe where and how the  $h$ -field has been computed, while the text on the RHS should provide the same information for the  $e$ -field. The slab is confined to the layers 0 and  $N$ . The  $e$ -fields outside the slab on the outermost layers are used to formulate the boundary conditions in terms of matrices  $\Phi_u$  and  $\Phi_l$ .

and  $h_n(z)$  appearing in (8), we can use  $e_n \exp(\lambda_n z)$  and  $h_n \exp(\lambda_n z)$ , respectively. Thus we have:

$$E_2(x, z) = \sum_{n=0}^{N-1} e_n e^{j(k_n+K)x} e^{\lambda_n z} \quad (22a)$$

$$H_1(x, z) = \sum_{n=0}^{N-1} h_n e^{j(k_n+K)x} e^{\lambda_n z}. \quad (22b)$$

We next substitute (22) into (7), and apply the functional  $D_m$  to the terms involved. Noting that  $\varepsilon$  is a constant, we have  $\varepsilon_{m-n}(z) = \delta[m-n]$ . Therefore, we obtain:

$$\frac{j}{\omega\mu} (k_n + K)^2 e_n - j\omega\varepsilon e_n = \lambda_n h_n \quad (23a)$$

$$-j\omega\mu h_n = \lambda_n e_n. \quad (23b)$$

Solving for  $h_n$  from (23b), and substituting the result into (23a) we arrive at

$$\frac{j}{\omega\mu} (k_n + K)^2 e_n - j\omega\varepsilon e_n = -\frac{\lambda_n^2}{j\omega\mu} e_n. \quad (24)$$

For nontrivial solutions we obtain  $(k_n + K)^2 - \omega^2\mu\varepsilon = \lambda_n^2$ . Or, equivalently,

$$\lambda_n = \pm \sqrt{(k_n + K)^2 - \omega^2\mu\varepsilon} = \pm w_n. \quad (25)$$

As the next step we establish a relationship between  $e^{-1/2}$  and  $h^0$  to formulate the boundary condition we are looking for. We use the fact that  $e_n^0 = e_n^{-1/2} e^{\lambda_n \Delta_z/2}$ . In free space Sommerfeld's radiation condition permits

only those fields which decay at infinity. This condition is met by taking the branch  $\lambda_n = w_n$ , as defined in (25). Then, we obtain  $e_n^0 = e_n^{-1/2} e^{w_n \Delta z/2}$ . From (23b) we obtain:  $h_n^0 = -(w_n/j\omega\mu)e_n^0$ . Using the last two equations we arrive at

$$h_n^0 + \frac{w_n}{j\omega\mu} e_n^{-\frac{1}{2}} e^{w_n \frac{1}{2} \Delta z} = 0. \quad (26)$$

This equation defines the desired ‘‘boundary’’ matrix  $\mathbf{C}^{-1/2}$  which relates  $e^{-1/2}$  to  $h^0$ . Analogously we obtain the ‘‘boundary’’ matrix  $\mathbf{C}^{n_z+1/2}$  which relates  $h_n^{n_z}$  to  $e_n^{n_z+1/2}$ . Proceeding similarly we obtain

$$h_n^{n_z} - \frac{w_n}{j\omega\mu} e_n^{n_z+\frac{1}{2}} e^{\frac{1}{2} \Delta z w_n} = 0 \quad (27)$$

which yields the desired boundary condition. Note that the resulting equality  $\mathbf{C}^{-1/2} = \mathbf{C}^{n_z+1/2}$  is an implication of  $\varepsilon^{-1/2} = \varepsilon^{n_z+1/2}$ .

### B. Inhomogeneous boundary problems

The scheme presented above is not restricted to homogeneous boundaries. Assume that the dielectric function outside the slab satisfies the following two conditions: for  $z < 0$  or  $z > h_z$  (i)  $\partial_z \varepsilon(x, z) \equiv 0$ , and (ii)  $\varepsilon(x + L_1) = \varepsilon(x)$ , where  $L_1$  is the periodicity length in the slab. For the fields we have the expansions:

$$E_2(x, z) = \sum_{m=0}^{N-1} f_m \sum_{n=0}^{N-1} e_{m,n} e^{j(k_n+K)x} e^{\lambda_m z} \quad (28a)$$

$$H_1(x, z) = \sum_{m=0}^{N-1} f_m \sum_{n=0}^{N-1} h_{m,n} e^{j(k_n+K)x} e^{\lambda_m z}. \quad (28b)$$

The constituent terms in these equations are built from the eigenvectors and the corresponding eigenvalues  $\lambda_m$  (the propagation constants in  $z$ -direction). In order to compute the desired eigenpairs, we substitute

$$E_2(x, z) = \sum_{n=0}^{N-1} e_n e^{j(k_n+K)x} e^{\lambda z} \quad (29a)$$

$$H_1(x, z) = \sum_{n=0}^{N-1} h_n e^{j(k_n+K)x} e^{\lambda z} \quad (29b)$$

into (7) and process the LHS of the equation as described in section III.A. This leads to an algebraic eigenvalue equation of dimension  $2N$  from which the desired eigenvalues and vectors can be solved numerically. Only eigenvalues which lead to decaying fields should be considered as explained above. This procedure is a generalization of the homogeneous boundary. In homogeneous case, the ‘‘boundary’’ matrices are diagonal because each eigenvector has only one non-zero element. In inhomogeneous case, the eigenvectors have in general  $N$  non-zero elements and the resulting boundary matrices are full.

## V. SOLVING LINEAR SYSTEMS OF THE EQUATIONS

In the preceding sections we explained the theoretical basis of our method. In the following we will describe how this theory can be applied to eigenmode and excitation problems. In addition we will explain how to solve the involved equation systems efficiently using iterative solvers.

### A. Excitation problems

In this section we consider an elementary excitation problem, which can be formulated in terms of the following interface condition for the magnetic field:

$$\lim_{\delta \rightarrow 0} h_1 \left( z^0 + \frac{\delta}{2} \right) - h_1 \left( z^0 - \frac{\delta}{2} \right) = \rho_2(z^0). \quad (30)$$

Here  $h_1(z)$  denotes the  $x$ -directional magnetic field component and  $\rho_2$  represents a  $y$ -directional elementary current element.

In order to discretize (30), consider a three-point central difference scheme:

$$h_1(k\Delta) + \Delta \left\{ \frac{\partial h_1}{\partial z} \right\} \Big|_{z=(k+\frac{1}{2})\Delta} = h_1((k+1)\Delta). \quad (31)$$

Next add one point to the system, at position  $((k+1)\Delta - \delta)$  where  $\delta$  is an infinitesimally small but finite number, and insert the dipole source  $\rho_2$  at location  $((k+1)\Delta - \frac{\delta}{2})$ . In view of (30) we can write (31) as

$$h_1(k\Delta) + \Delta \left\{ \frac{\partial h_1}{\partial z} \right\} \Big|_{z=(k+\frac{1}{2})\Delta} + \rho_2 = h_1((k+1)\Delta). \quad (32)$$

As a generalization, we can substitute the  $x$ -directional Fourier expansion in place of the scalar variables above. Evaluating the derivative as in (12a) and writing the terms using the notation of (21) we obtain

$$h_k - h_{k+1} + B'_{k+\frac{1}{2}} e_{k+\frac{1}{2}} = -\rho_{k+\frac{1}{2}}. \quad (33)$$

Obviously the mere difference between this equation and (21b) is the excitation term at the RHS. In (33) the excitation has been indexed by  $(k + \frac{1}{2})$  due to the finite resolution in our discretized system: We cannot specify the position of the dipole source more precisely than stating that it is located somewhere between the layers  $k$  and  $(k+1)$ .

From the above discussion it can be concluded that for solving excitation problems we merely need to replace the zero vector at the RHS of (21b) by the Fourier transform of the current distribution. A similar procedure can be conducted *mutatis mutandis* for the determination of electric fields due to magnetic currents.

The discretized inhomogeneous system of equations describing the present excitation problem has the form

$$\mathbf{A}(\omega, \mathbf{K})\mathbf{x} = \mathbf{b}(\omega, \mathbf{K}) \quad (34)$$

where  $\mathbf{x}$  represents the unknown coefficient vector and  $\mathbf{b}$  is the excitation vector. The solution to this problem can be obtained by using standard techniques, e.g. LU-decomposition or Gauss elimination, unless matrix  $\mathbf{A}$  is singular, in which case we recommend to resort to one of the techniques described below.

Once the solution to (34) has been obtained, we use (8) to construct the fields in real domain. As pointed out earlier, the expansions of the fields are simply Fourier transforms with respect to  $x$  on various layers  $z = i\Delta$ . Therefore, we can synthesis the fields from the coefficients merely by applying the inverse Fourier transform.

### B. Eigenstate problems

1) *Theorem:* A homogeneous linear system

$$\mathbf{A}\mathbf{x} = \mathbf{0} \quad (35)$$

always has the trivial solution  $\mathbf{x} = \mathbf{0}$ . Nontrivial solution exist if and only if  $\text{rank}(\mathbf{A}) < \mathbf{n}$ . If  $\text{rank}(\mathbf{A}) = \mathbf{r} < \mathbf{n}$ , these solutions, together with  $\mathbf{x} = \mathbf{0}$ , form a vector space of dimension  $n - r$ .

One way to determine the rank of a matrix is to count all its eigenvalues which are equal to zero. The corresponding eigenvectors expand the null space of  $\mathbf{A}$  among which we can construct all the solutions.

This information can also be obtained through singular value decomposition. If  $n$  singular values are zero, then the null space of  $\mathbf{A}$  has dimension  $n$  and the equation system has a solution of degeneracy  $n$ .

A more efficient way to investigate the singularity of a matrix is to perform an LU-decomposition and calculate its determinant by multiplying the diagonal elements of the upper diagonal matrix. The determinant itself is generally inappropriate for determining the singularity of a matrix due to the lack of a uniform scale: The determinant can be very large even if the matrix is nearly singular or vice versa. In our case it does not really matter much since we are aiming at ratios. We construct the system matrix for consecutive  $\omega$  values and compare the associated determinants. For  $\omega$ 's near a singularity, the value of the determinant drops sharply and we can iterate towards the resonant frequency. In the next session we address the details of the iterative scheme used.

### C. Iterative solver

For large problems, iterative rather than direct solvers should be considered since they often significantly speed up the computations. Our choice for it-

erative solver has been the Transpose Free Quasi Minimal Residual method (TFQMR), which is a Krylov-subspace method for non-Hermitian matrices [3]. It is efficient, tolerant against breakdowns, and handles singular matrices well.

TFQMR (as many other iterative solvers) only requires products by the matrix to be solved and, thus, the matrix never actually has to be constructed. All is needed is a routine that returns the product of the matrix by a given trial vector.

1) *Generating matrix products:* The operator in (7a) has two parts: the spatial derivatives and a multiplication by a function  $\varepsilon$  in the spatial domain. Derivatives are trivially simple to compute in the Fourier domain as they reduce to algebraic multiplication by the respective Fourier expansion term. On the other hand, multiplication by  $\varepsilon$  leads to a convolution - or - in discretized version, to a multiplication by a convolution matrix (18). It is known from the theory of Fourier transforms that convolution in Fourier domain corresponds to a multiplication in real domain and vice versa. Therefore, the convolution can be evaluated by inverse Fourier transforming the coefficient matrix, multiplying by  $\varepsilon$  in the real domain, and finally Fourier transforming back. This approach is justifiable because multiplication by the (full) convolution matrix is an  $O(N^3)$  operation for  $N$  coefficients, but in real domain, we multiply spatial fields with the corresponding  $\varepsilon$ , requiring only  $O(N)$  operations. Dominating factor,  $O(N \ln(N))$ , comes from the FFT.

This approach can not be used in constructing the system matrix  $\mathbf{A}$ , it is only amenable to evaluating matrix vector products.

2) *Preconditioning:* The convergence rate of iterative methods decisively depends on the matrix they are applied to. Occasionally, they may completely fail to converge. However, instead of solving  $\mathbf{A}\mathbf{x} = \mathbf{b}$  we can solve the equivalent form

$$\mathbf{M}_1^{-1}\mathbf{A}\mathbf{M}_2^{-1}(\mathbf{M}_2\mathbf{x}) = \mathbf{M}_1^{-1}\mathbf{b} \quad (36)$$

for the new unknown vector  $\mathbf{y} = \mathbf{M}_2\mathbf{x}$  and the RHS  $\mathbf{c} = \mathbf{M}_1^{-1}\mathbf{b}$ . Our expectation is that the solver may converge faster for the new matrix  $\mathbf{M}_1^{-1}\mathbf{A}\mathbf{M}_2^{-1}$ . The primary objective is then to find suitable preconditioner matrices  $\mathbf{M}_1$  and  $\mathbf{M}_2$  such that their inverse can be computed with a reasonable effort, and that they would transform the matrix into a nearly diagonal one. To this end various standard techniques have been developed, e.g. partial LU-decomposition, but we decided to use a problem-specific strategy in which relevant information from  $\mathbf{A}$  is used. In our case we use only one sided preconditioning and set  $\mathbf{M}_1 = \mathbf{I}$ . The right preconditioner matrix  $\mathbf{M}_2$  is constructed from three diagonals of  $\mathbf{A}$ . In effect,  $\mathbf{M}_2$  corresponds to a system matrix of a modified problem in which  $\partial_x \varepsilon(x, z) \equiv 0$ . The discretized dielectric function for the ‘‘reduced’’

problem can be obtained by averaging the original dielectric function on each  $z$ -layer,  $\epsilon_k = \text{ave}(\epsilon_k)$ , over one period.

We do not invert  $\mathbf{M}_2$  explicitly. Instead, we solve  $\mathbf{M}_2 \mathbf{z} = \hat{\mathbf{y}} \Rightarrow \mathbf{z} = \mathbf{M}_2^{-1} \hat{\mathbf{y}}$ , where  $\hat{\mathbf{y}}$  is a trial vector given by TFQMR. After this,  $\mathbf{z}$  is multiplied by  $\mathbf{A}$  as explained above and the result is returned TFQMR. The linear system concerning  $\mathbf{M}_2$  can be solved efficiently using Gauss elimination because there are non-zero elements only on three diagonals. The elements of  $\mathbf{M}_2$  are computed once for each different  $\mathbf{A}$  and then reused in the subsequent iterations.

3) *Iterative solution of Solving eigenstates*: Eigenstates can also be solved iteratively as will be demonstrated in section VI. This technique does not involve matrix factorization directly nor the computation of its determinant. Consider the following system

$$\mathbf{A}(\omega, \mathbf{K})\mathbf{x} = \mathbf{y} \quad (37)$$

where  $\mathbf{y}$  is some non-zero vector, while the remaining terms are defined as before. This is an inhomogeneous system and can be solved using the iterative technique described above. If  $\mathbf{A}(\omega, \mathbf{K})$  approaches a singular point, then  $\mathbf{x}$  approaches an eigenvector of  $\mathbf{A}(\omega, \mathbf{K})$  corresponding to an eigenvalue 0, nearly independently of  $\mathbf{y}$ . Furthermore, the norm of the solution  $\mathbf{x}$  approaches infinity. The proof of this statement and limitations on the choice of  $\mathbf{y}$  are provided in [4]. This property can be used as a measure for matrix singularity in place of, e.g. the determinant.

In many instances iterative solutions are preferred since they require less computer resources than the direct factorization of the matrix, and, at the same time, give the field solution.

## VI. NUMERICAL RESULTS

We solve dispersion diagrams for two problems and compare results with those obtained by a planewave method (PWM) [5]. In addition, we present field solutions for a third problem, which consists of a slab with Gaussian dielectric profile function. We use TFQMR to find the field solution due to a single dipole excitation. Our objective is to find the singular points of the system matrix where the solution norm approaches infinity. Because it is easier to search zeros rather than infinities we use an ‘‘inverted’’ form instead. Then our objective function becomes  $F(\omega) = (\|\mathbf{A}^{-1}(\omega)\mathbf{b}\|_2)^{-1/2}$  where  $\mathbf{A}(\omega)$  is the system matrix and  $\mathbf{b}$  is the excitation vector. The minimization takes place in two steps: first we bracket the minimum between two points and then we decrease the interval to the desired accuracy. When bracketing the minimum, we fit a second order polynomial to three points of  $F(\omega)$  in order to estimate the location of a fourth point. This allows us to adapt the step size according to the derivative and absolute value

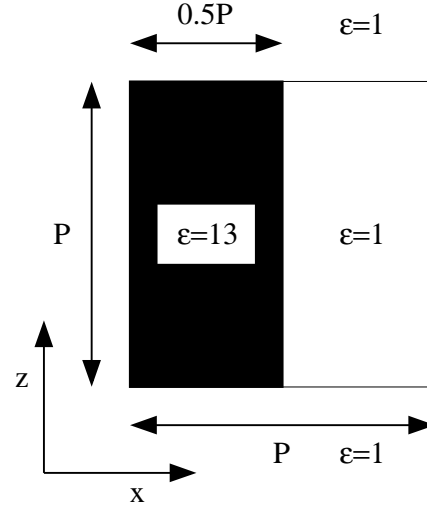


Fig. 2. One unit cell of the test structure 1. The structure is periodic in  $x$ -direction with period  $P$ . Above and below the slab, as well as the space between the corrugation is free space.

of  $F(\omega)$  and therefore take great leaps away from the minimum and small steps in its vicinity. When the minimum has been bracketed, we switch to golden section search in order to decrease the bracketed interval.

In the planewave method, the problem is assumed to be periodic in all directions. Therefore, in order to apply this technique, we need to periodize the structure artificially by adding sufficiently large free space in the  $z$ -direction. The resulting enlarged unit cell, i.e. a supercell, is then periodized. This approach is justifiable if the modes are confined around the slab in  $z$ -direction, such that immediate neighboring supercells have negligible interaction. This can be verified by repetitively solving the problem with larger and larger supercell until the results converge.

### A. A slab with rectangular corrugation

Our first test case is a slab with a periodic and rectangular corrugation. The period is  $L_1 = P$ , the height of the slab  $h = P$  and the pitch-to-mark ratio is 0.5 ( $l = 0.5P$ ). The relative dielectric constant of the slab is  $\epsilon = 13$ . Above and below the slab, as well as, the space between the corrugation is free space. A schematic picture of the structure is presented in Fig. 2.

In order to apply the planewave method we have used a supercell with dimensions  $L_1 = P$  and  $L_z = 12P$ . The computed dispersion diagram is shown in Fig. 3. Red curves with circular markers are obtained using our method, while blue lines with cross markers have been computed using the planewave method. The thick black line indicates the lightline, above which modes are radiating. Note that due to the artificial periodiza-

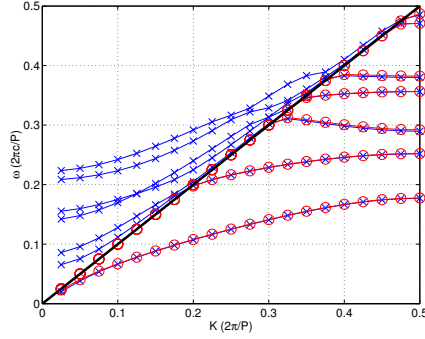


Fig. 3. Dispersion diagram for a slab with rectangular corrugation. Red lines with circular markers are computed using our method, while blue lines with cross markers have been computed using plane wave method. In our method we used 64 planewaves in  $x$ -direction and 64 finite differences in  $z$ -direction. For the plane wave method we used 64 planewaves in a unitcell; i.e.  $64 \times (12 \times 64)$  planewaves all together.

tion in the plane wave method, even unbounded modes appear guided.

This is an artifact, which is avoided in our method: For weakly or nonguided modes the interaction between consecutive supercells is no longer negligible and, therefore, they appear guided.

### B. A slab with cylindrical corrugation

Our second test case is a similar slab but this time with a cylindrical corrugation. The slab dimensions, material, period length and discretization scheme are as above. However, the corrugation is formed of  $y$ -directional air cylinders (voids) with  $r = 0.4P$ . The structure is shown in Fig. 4.

Because the discretization is rectangular in both methods, we have averaged  $\varepsilon$  in the boundary cells in order to bring the average closer to its true value. The computed dispersion diagram is shown in Fig. 5.

### C. Field solution in a slab with Gaussian dielectric profile

Our third test case is a slab with thickness  $h_z = 1$  and  $x$ -directional periodicity  $L_1 = P = 1$ . The dielectric function in the fundamental unit cell of the slab is

$$\varepsilon(x, z) = 1 + 9e^{-\left(\frac{0.5-x}{0.2}\right)^2} e^{-\left(\frac{0.5-z}{0.2}\right)^2}. \quad (38)$$

Above and below the slab is free space. The dispersion diagram, which shows that this slab supports two TE-polarized modes, is presented in Fig. 6.

We solved the fields resulting from one  $y$ -directional dipole located at  $(x, z) = (0.30, 0.27)$  for  $(K, \omega) = (0.4, 0.2816)$ . As can be seen from the dispersion diagram, this point corresponds to an eigenfrequency of the system and, therefore, the system matrix is (nearly)

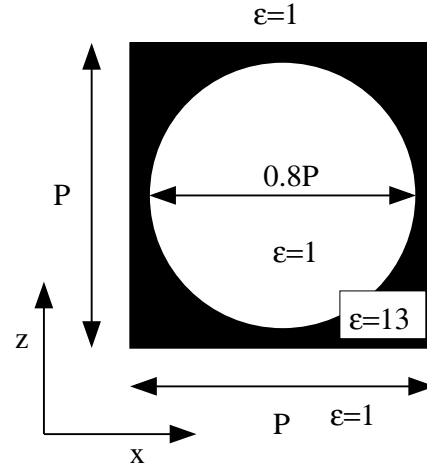


Fig. 4. One unit cell of the test structure 2. The structure is periodic in  $x$ -direction with period  $L_1 = P$ . Above and below the slab in  $z$ -direction, we assume free space.

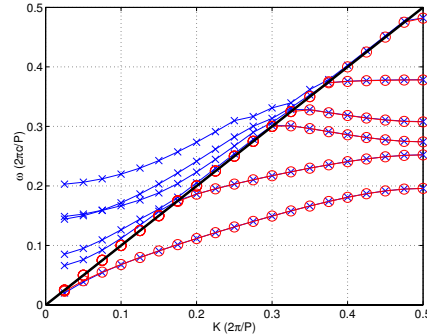


Fig. 5. Dispersion diagram for a slab with cylindrical corrugation.

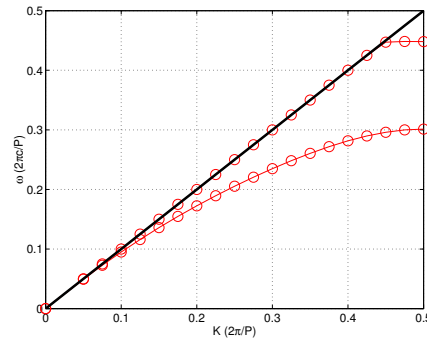


Fig. 6. Dispersion diagram for a slab with a Gaussian dielectric function as computed by our method.

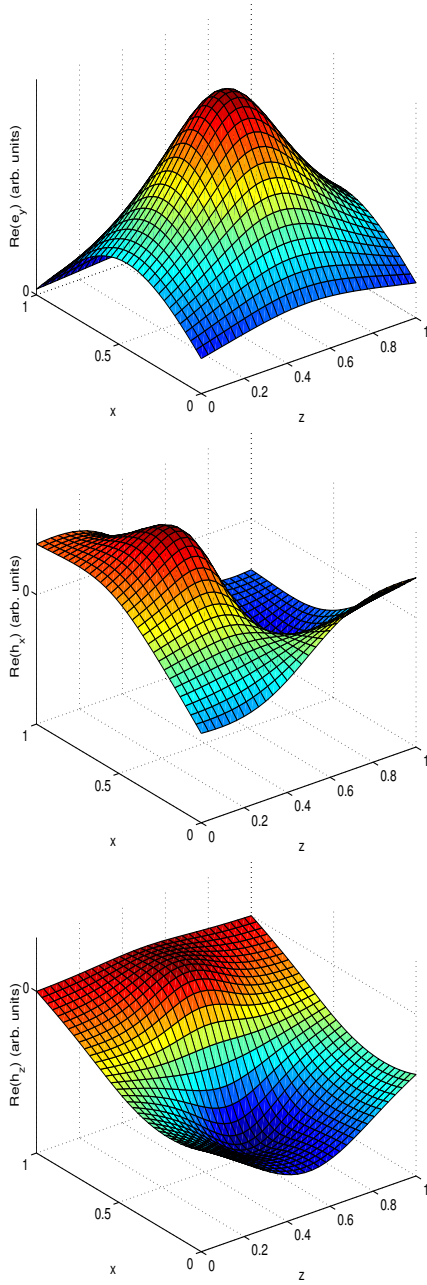


Fig. 7. Real part of eigenmode fields for a slab with Gaussian dielectric function, computed for  $(K, \omega) = (0.4, 0.2816)$ .

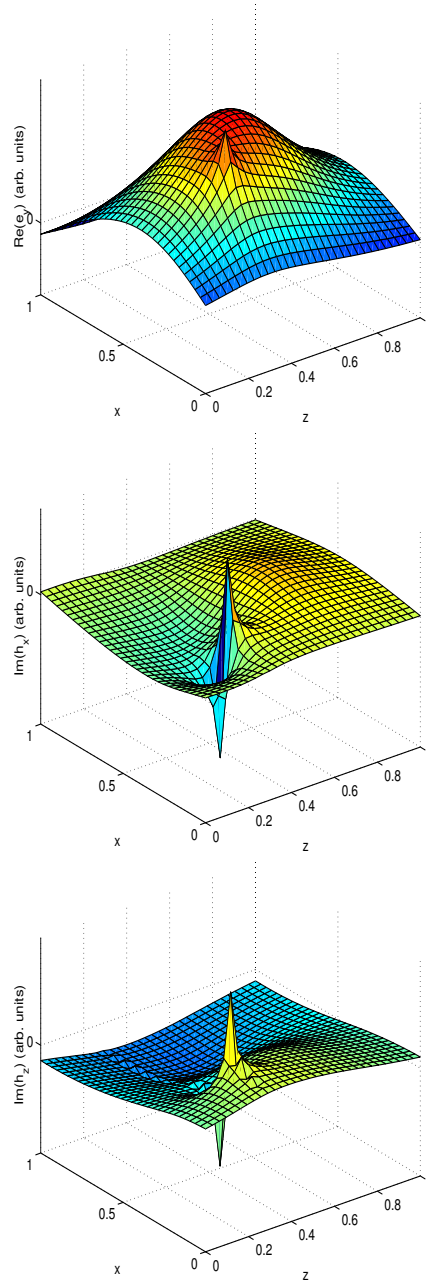


Fig. 8. Fields in a slab with Gaussian dielectric function, computed for  $(K, \omega) = (0.5, 0.2816)$ .

singular. Field distributions  $e_2$  and  $h_1$  presented in Fig. 7 are the transversal field components obtained directly by solving (34). Whereas the orthogonal field component  $h_3$  is computed *a posteriori* using (5b). In the field patterns there is no trace of the dipole excitation. This can be understood as follows: A dipole excitation pumps energy into a resonating system and, therefore, the energy grows without bounds, until the excitation is negligible compared with the field strength. Mathematically speaking, the system matrix  $\mathbf{A}$  has an eigenvalue 0 and, therefore, the solution of (34) is in the space which is spanned by eigenvectors corresponding to an eigenvalue 0. A more formal proof is given in [4].

Fields in response to an excitation in the same location but obtained for  $(K, \omega) = (0.5, 0.2816)$  are shown in Fig. 8. Now the dipole excitation is clearly visible in the field patterns. Moreover, the ratio of field peak values at eigen frequency and this frequency, as returned by the iterative solver, is of order  $10^8$ .

## VII. DISCUSSION OF THE NUMERICAL RESULTS AND CONCLUSIONS

### A. Searching for the minimum

The computational effort needed to solve the eigenmodes depends on how efficiently the system equation can be solved and how many times it has to be done. We have already addressed how accelerate the solver, here we discuss how minimize  $F(\omega)$  efficiently for a given  $K$ . Currently we fit a second order polynomial to three previously computed points in order to estimate the location of the fourth one. When the curve approaches a minimum we decrease the step size trying to avoid overshooting the minimum. Practice has shown that it is good to aim at a point that changes the norm by 10% compared to the previous value. It is tempting to use bigger steps but then we risk jumping over a minimum without noticing its occurrence. This is especially crucial for closely spaced modes. Smaller steps on the other hand are more secure but then we end up solving the fields in unnecessarily many  $\omega$  points. A typical search pattern is shown in Fig. 9.

When the minimum is bracketed, we switch to golden section search to iterate the minimum to the desired accuracy. The advantage of this procedure is that golden section search converges at a predetermined rate and it does not suffer from lock ups. The disadvantage is that the convergence rate is predetermined even though we could perform better since we have a good idea of the curve behavior. Most of the standard minimization techniques are not applicable because they assume parabolic behavior near the minimum. Instead, we could fit polynomials to both sides of the minimum and increase the degree as more points are solved. The crossing of the two polynomials would then be the next search point. However, this method is prone to lock ups

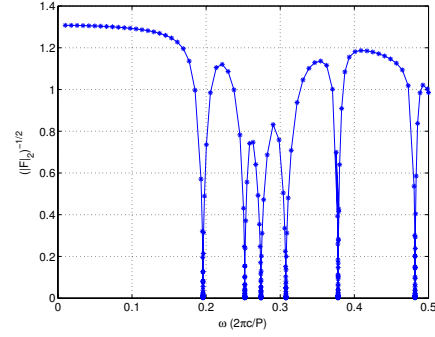


Fig. 9. Field energy function  $F(\omega)$  for the test case with cylindrical corrugation. The phasing factor is chosen to be  $K = 0.5$  (in Brillouin zone units). The behavior is very regular allowing efficient optimization techniques in the quest for minima.

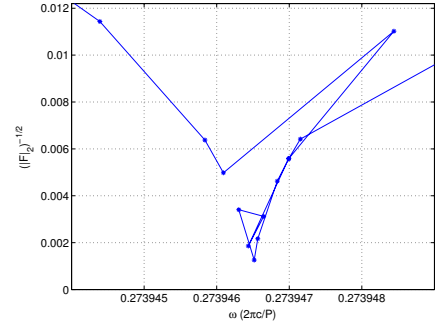


Fig. 10. Search pattern in the vicinity of the minimum for the third order mode with  $K = 0.5$  (in Brillouin zone units) of the slab with cylindrical corrugation.

and has not been experimented so far. A typical search pattern in the vicinity of a minimum is shown in Fig. 10.

### B. Convergence

1) *Convergence of the iterative solver:* It is difficult to make precise statements for the convergence behavior of the iterative solver because it strongly depends on a variety of parameters. With our preconditioner, the number of iterations needed usually varies between 2 and 20. Key factors are the dielectric function and the condition number of the matrix. In addition, the initial guess has an influence, even though a minor one.

Typically problems with  $\partial \varepsilon(x, z) / \partial x$  being small converge fairly quickly. This is because large variations of  $\varepsilon$  in  $x$ -direction create large off-diagonal terms in the system equation. The three-diagonal preconditioner is capable of directly solving a matrix with only three diagonals but all off-diagonal terms are left for the it-

erative solver. Therefore, the bigger the off-diagonal terms are, the worse is the condition number of the preconditioned matrix and the more iterations are needed by the iterative solver. It is worth mentioning that if  $\partial\varepsilon(x, z)/\partial x = 0$ , there are no elements outside the three diagonals in the system matrix and only one application of the preconditioner solves the problem. No iterations are needed. It should also be pointed out that because of the finite difference approach in  $z$ -direction,  $\partial\varepsilon(x, z)/\partial z$  has no effect on convergence. All variations with respect to  $z$  are eliminated by the preconditioner.

It appears that the condition number of the matrix is also a factor in the iterative solver convergence. This is unfortunate since the eigenmodes of the system are found exactly in the singular points of the system matrix. The effect is not dramatic; the number of the iterations required for convergence is maybe four fold as compared to a well behaved point, all other factors being held equal. Again, it is rather difficult to make precise statements because other factors often have a more significant effect. As an example, in the cylindrical-void slab problem with  $n_x = n_z = 64$ , convergence at  $K = 0.5$ ,  $\omega = 0.1$  requires three iterations (TFQMR requires two matrix products for each iteration) and at the lowest order eigenmode -  $K = 0.5$ ,  $\omega = 0.195719$  - 12 iterations are needed.

The number of discretizations, on the other hand, does not have a direct effect on convergence. Solving the above mentioned problem with  $n_x = n_z = 384$ , requires three and eleven iterations, respectively.

2) *Convergence of eigenfrequencies:* Our method gives precise results with a small number of discretization steps. As an example, we analyze the slab problem with cylindrical corrugation. We have solved the lowest order eigenfrequency for  $K = 0.5$  with both, our method, and the planewave method, increasing discretization until the results converged. The convergence behavior is shown in Fig. 11.

In conclusion we summarize the distinct properties of our method: The difference between converged frequencies for  $n = 16$  and  $n = 384$  is only 0.024%. The relative difference between converged frequencies as solved with our method and the planewave method for  $n = 384$  is 0.00204%.

## VIII. ACKNOWLEDGEMENTS

This work was partially done while the second author (A. R. Baghai-Wadji) was visiting the Institute for Mathematical Sciences, National University of Singapore and Institute for High Performance Computing (IHPC) in 2003. This visit was supported by the Institute and IHPC.

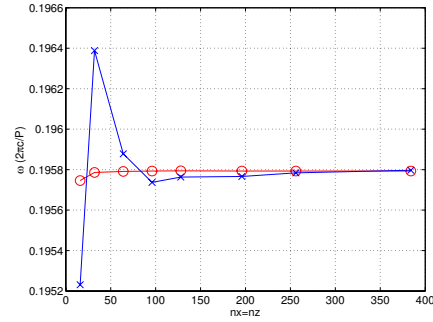


Fig. 11. Shows the lowest order eigenfrequency of  $K = 0.5$  point for the slab with cylindrical corrugation as a function of the number of discretization points. Red curve with circular markings is the frequency as solved by our method, and blue with cross markings obtained by the planewave method.  $x$ -axis represents the number of discretization steps within one unit cell (same in both  $x$ - and  $z$ -directions). For the planewave method, the number of planewaves in  $z$ -direction is  $12n_z$  compensating the size of the supercell. Therefore both methods have equally many discretization points within the unit cell area.

## REFERENCES

- [1] K. Varis, A.R. Baghai-Wadji, "Hybrid Planewave/Finite-Difference Transfer Method for Solving Photonic Crystals in Finite Thickness Slabs," Proceedings EDMO, Electron Devices for Microwave and Optoelectronic Applications, pp. 161-166, Vienna University of Technology, Vienna, Austria, 15-16 November, 2001.
- [2] K. Varis, A.R. Baghai-Wadji, "A Novel 3D Pseudo-spectral Analysis of Photonic Crystal Slabs," ACES journal, **19**, no. 1 b, pp. 101-111, 2004.
- [3] R. W. Freund, N. M. Nachtigal, "A Transpose-Free Quasi-Minimal Residual Algorithm for Non-Hermitian Linear Systems," SIAM Journal on Scientific Computing, **14**, pp. 470-482, 1993.
- [4] W. H. Press, S. A. Teukolsky, W. T. Vetterling, B. P. Flannery, "Numerical recipes in C: the Art of Scientific Computing, 2nd Ed.," Cambridge University Press, Cambridge, pp. 493-495, 1992.
- [5] S. G. Johnson, J. D. Joannopoulos, "Block-Iterative Frequency-domain Methods for Maxwell's Equations in a Planewave Basis," Optics Express, **8**, no. 3, pp. 173-190, 2001.



**Karri Varis** was born in Espoo, Finland, in 1974. He received a M.Sc. degree in Electrical Engineering from Helsinki University of Technology in 1999. Since then, he has been a doctoral student in the Finnish Graduate School of Modern Optics and Photonics and working in the Optoelectronics Laboratory,

Helsinki University of Technology. His current research interest includes the enhancement and development of computational techniques for the analysis of periodic and non-periodic systems, with an emphasis on photonic crystals and optical devices.

**Ali R. Baghai-Wadji** was born in Marand, Iran, on May 6, 1953. He has been with the Electrical Engineering and Information Technology Department at Vienna University of Technology (VUT), Vienna, Austria, since 1979. From 1979 to 1984 he was an associate researcher in Physical Electronics and Applied Electronics Groups, where he developed computer models for microelectronic and microacoustic devices. He earned his M.Sc. and Ph.D. in electrical engineering in 1984 and 1987, respectively, and obtained his *venia docendi* in physical electronics in 1994, all from VUT. Since 1997 he has been an associate professor at VUT. Currently he is heading the Accelerated Computational Technology (ACT) Group at the Institute for Fundamental and Theory of Electrical Engineering at VUT. Three times he was awarded the Kurt Gödel research scholarship from Austria, allowing him to spend a total of 10 months at UCI, University of California, Irvine, during the years 1990, 1991, and 1992. From 1994 to 1999 he was, on leave of absence from VUT, a principal engineer consultant in the United States serving more than four years for Motorola, Government System and Technology Group, Scottsdale, Arizona, and nearly one year for CTS-Wireless components in Albuquerque, New Mexico. In 1999 and 2000 he was (15 months) a visiting professor at Materials Science Laboratory, Helsinki University of Technology (HUT). That professorship was awarded by Nokia Research Foundation, and TEKES, a national science foundation in Finland. In addition, in the Fall 2000 he was awarded a Nokia Visiting Fellowship. In 2003 he was awarded a *venia docendi* for modeling and simulation of classical and quantum electronic devices and materials at HUT for an initial period of 6 six years. In 2003 he was four months an invited senior member of the Institute for Mathematical Sciences, and a visiting professor at the Institute for High Performance Computing, in Singapore. Since 1995 he has also been affiliated with Arizona State University as an adjunct professor at the Department for Mathematics and Statistics. In 2002 he was elected an honorary member of the Electromagnetics Academy, Massachusetts, USA. He has supervised five PhD dissertations, and eleven Masters' theses. He has lectured 12 short courses at various IEEE conferences internationally. He has authored more than 120 publications in reviewed journals and conference proceedings, and has one patent. His current research interest includes the development of accelerated computational modeling techniques, quantum mechanics, photonic crystals, and molecular electronics. Since 1995

he has been a senior member of the IEEE, an IEEE-UFFC associate editor, and an IEEE-UFFC technical program committee member. He was the guest editor for a special issue on *Modeling, Optimization, and Design of Surface and Bulk Acoustic Wave Devices* in IEEE Transactions on Ultrasonics, Ferroelectrics, and Frequency Control (Sept. 2001, Vol. 48, Num. 5). He has been appointed the general chairman of the PIERS'5 conference.